Improved Performance of Molecular Bulk-Heterojunction Photovoltaic Cells through Predictable Selection of Solvent Additives

*Kenneth R. Graham, Patrick M. Wieruszewski, Romain Stalder, Michael J. Hartel, Jianguo Mei, Franky So, and John R. Reynolds**

Solvent additives provide an effective means to alter the morphology and thereby improve the performance of organic bulk-heterojunction photovoltaics, although guidelines for selecting an appropriate solvent additive remain relatively unclear. Here, a family of solvent additives spanning a wide range of Hansen solubility parameters is applied to a molecular bulk-heterojunction system consisting of an isoindigo and thiophene containing oligomer as the electron donor and [6,6]-phenyl-C_{61}-butyric acid methyl ester ($PC_{61}BM$) as the electron acceptor. Hansen solubility parameters are calculated using the group contribution method and compared with the measured solubilities for use as a screening method in solvent additive selection. The additives are shown to alter the morphologies in a semipredictable manner, with the poorer solvents generally resulting in decreased domain sizes, increased hole mobilities, and improved photovoltaic performance. The additives with larger hydrogen bonding parameters, namely triethylene glycol (TEG) and *N*-methyl-2-pyrrolidone (NMP), are demonstrated to increase the open circuit voltage by ~0.2 V. Combining a solvent additive observed to increase short circuit current, poly(dimethylsiloxane), with TEG results in an increase in power conversion efficiency from 1.4 to 3.3%.

1. Introduction

Organic photovoltaics (OPVs) are emerging as a promising alternative to their more costly inorganic counterparts, with rapidly increasing efficiency values and a corresponding increase in research efforts.[1–7] Specifically, solution processed bulk-heterojunction (BHJ) OPVs have attained power conversion efficiencies (PCEs) in excess of 7% by utilizing conjugated polymers as the electron donors (D) and fullerene derivatives as the electron acceptors (A).[4–7] Alternatively, the more recently developing solution processed molecular BHJ OPVs have obtained PCEs of 4 to 6%,[8–11] where a conjugated small molecule replaces the conjugated polymer as the electron donor.

In both polymer and molecular based BHJ OPVs, the morphology of the D/A blend is of critical importance to their efficient operation.[12–13] The excitons generated on the D and A phases must be able to diffuse to a D/A interface where they can dissociate into free electrons and free holes. An interconnected network of D and A phases is then required for transport of the electron or hole to the electrode. Additionally, the hole and electron mobilities must be sufficiently high to allow for efficient charge transport. Given these requirements and typical organic exciton diffusion lengths, a phase separated morphology consisting of interpenetrating and interconnected D and A domains that are on the order of 10–30 nm is thought to be ideal for efficient device operation.[14,15] Furthermore, the D and A phases should consist of only D or A molecules and exhibit a high degree of order to reduce electron-hole recombination and provide higher mobilities.

The above listed requirements for efficient BHJ OPV operation has resulted in the application of various processing techniques directed at creating this optimal blend morphology. These techniques primarily include the use of appropriate casting solvents,[16–17] thermal annealing,[3] solvent annealing,[18,19] and the addition of relatively small amounts of high boiling point solvents referred to as solvent additives (SAs).[5,11,20–27] Recently, the use of SAs has become more widely adopted with significant improvements in PCE observed. These increases in PCE are attributed to the more optimal blend morphology achieved upon addition of the additive; however, the same additive may have distinctly different effects on systems based on different materials. For example, in the cases of P3HT:$PC_{61}BM$[20–22]

Dr. K. R. Graham, P. M. Wieruszewski, Dr. R. Stalder, Dr. J. Mei, Prof. J. R. Reynolds
The George and Josephine Butler Polymer Research Laboratory
Department of Chemistry and Center for Macromolecular Science and Engineering
University of Florida
Gainesville, FL 32611-7200, USA
E-mail: Reynolds@chemistry.gatech.edu
M. J. Hartel, Prof. F. So
Department of Materials Science and Engineering
University of Florida
Gainesville, FL 32611, USA
Prof. J. R. Reynolds
School of Chemistry and Biochemistry
School of Materials Science and Engineering
and Center for Organic Photonics and Electronics
Georgia Institute of Technology
Atlanta, GA 30332-0400, USA

DOI: 10.1002/adfm.201102456

and PCPDTBT:$PC_{71}BM$[24–26] the addition of 1,8-diiodooctane (DIO) or 1,8-octanedithiol results in increased crystallinity and increased D and A domain sizes, whereas in the cases of PDPPTPT:$PC_{61}BM$,[13] PTB7:$PC_{71}BM$,[27] and PDTSTPD:$PC_{71}BM$[5] the addition of DIO drastically reduces D and A domain sizes. These differing morphologies are attributed to the varying interactions of the SA with the different polymers, although a thorough study exploring the relationships has not yet been performed. Regardless of a complete mechanistic understanding, it is evident that SAs provide an effective means for controlling morphology and significantly increasing PCEs.

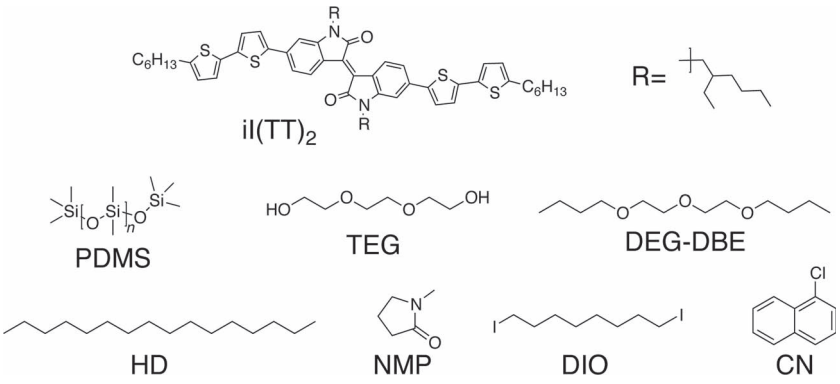

Scheme 1. Molecular structure of $iI(TT)_2$ and SAs used in processing photovoltaic cells.

The use of SAs has seen a more limited application to molecular BHJ OPVs, with reports of their use only appearing within the last year and, to the best of our knowledge, there are only three reports appearing to date.[11,28,29] In one case, the use of 1,8-octanedithiol has been demonstrated to increase the surface roughness and improve the short circuit current density (J_{SC}) when used with a triarylamine, thiophene, and benzothiadiazole containing small molecule blended with $PC_{71}BM$.[28] In another example, DIO is used to decrease the domain sizes, increase the J_{SC}, and increase the fill factor, thereby resulting in an increase in PCE from 4.5 to 6.7%.[11] Additionally, our group recently reported on the use of a macromolecular additive, poly(dimethylsiloxane) (PDMS), as a means to decrease surface roughness and domain size, which resulted in an increased PCE for a thiophene and isoindigo containing small molecule blended with $PC_{61}BM$.[29] Herein, we further investigate the influence of PDMS on film morphology and device performance, while also seeking to understand the mechanism for improvement and thereby identify guidelines for selecting appropriate SAs for use in molecular BHJ OPV cells.

To predict solubilities and thus provide a guideline for SA selection, this work utilizes the previously developed Hansen solubility parameters.[30] These solubility parameters have also recently been used by the Nguyen group to help in selecting an appropriate casting solvent for molecular BHJ OPVs.[17] Hansen solubility parameters are known for a large number of solvents and can be roughly calculated for most molecules using a straightforward method based on group contribution theory.[30,31] These solubility parameters are calculated for the thiophene and isoindigo containing oligomer, $iI(TT)_2$ as shown in **Scheme 1**, and $PC_{61}BM$ as a guide for SA selection. A family of seven solvents with widely varying Hansen solubility parameters, over which $iI(TT)_2$ and $PC_{61}BM$ display solubilities spanning a range of four orders of magnitude, are compared as SAs for the $iI(TT)_2$:$PC_{61}BM$ blend system. Small quantities (≤1 mg/mL) of the additives are observed to significantly alter the OPV device performance, hole and electron mobility, and blend morphology. Interestingly, the poor solvents for both $iI(TT)_2$ and $PC_{61}BM$ lead to smaller D and A domains with generally increased hole mobilities, where as better solvents lead to increased D and A domain sizes with hole mobilities less than the device with no additive. Consequently, the devices processed with poor SAs generally show an increased or unchanged PCE, while those processed with the better solvents show a decreased PCE relative to the cells without any SAs.

In the course of this planned morphology study, it was observed that the additives with high hydrogen bonding parameters result in increased open circuit voltages (V_{OC}) of ≈0.2 V over devices with no additives. This phenomenon is investigated and it is shown that an optimal device can be obtained by employing two additives simultaneously in the active layer processing solution, one to increase the V_{OC} with a second to increase the J_{SC}. The effect of additives on the V_{OC} is compared to the effect of substituting PEDOT:PSS for the higher work function material MoO_3. The influence of electrode material and the addition of TEG on the built-in voltage is probed through electroabsorption measurements, with results showing a 0.07 and 0.22 V increase in the built-in voltage upon addition of TEG and upon substitution of PEDOT:PSS for MoO_3 respectively.

2. Results and Discussion

2.1. Solubilities

The morphology of a multicomponent organic molecular or polymeric film is known to correlate with the degree of interaction between the various materials in the film and the interactions of the materials with the solvent(s).[17,32] For example, if the materials have unfavorable interactions towards one another they tend to display much larger degrees of phase separation. Additionally, the relative solubility of each material in the solvent significantly influences the film morphology, with phases increasing in size as the solubility difference increases.[17,32] To aid in predicting molecular interactions and thereby solubilities, several different numerical methods have been developed.[30,31,33]

The square root of the cohesive energy density, defined as the enthalpy of vaporization divided by the molar volume, is commonly known as the Hildebrand solubility parameter and provides one of the most basic and fundamental numerical estimators of molecular interactions and therefore solubilities.[33] Although it provides a useful estimate, it is only a single term resulting from the total interaction forces and can be misleading

Table 1. Calculated Hansen solubility parameters for $iI(TT)_2$ and $PC_{61}BM$ based on the group contribution method.

Solvent	Hansen Solubility Parameters[a)]		
	δ_D	δ_P	δ_H
$iI(TT)_2$	21.7	2.9	4.7
$PC_{61}BM$	20.6	2.4	3.5

[a)]Group contribution values taken from Barton[31] with exception of C_{60} group which was taken from Hansen and Scott.[35] All units are $MPa^{1/2}$.

in predicting the behavior of systems where different intermolecular interactions exist. Consequently, the Hansen solubility parameters were later developed which essentially break the Hildebrand solubility parameter into dispersion (δ_D), polar (δ_P), and hydrogen bonding (δ_H) terms.[30,34] The more similar these terms are, the more favorable the interactions and the more miscible two solvents will be, the more soluble a material will be, and the less thermodynamic driving force for phase separation. As shown in Equation 1, one term which quantifies this difference is the distance between the two components in Hansen solubility space, *Ra*, which will be used here as an indication of the predicted solubility.[30] Larger values of *Ra* indicate that the molecules are further apart in solubility space and molecular interactions will be more unfavorable.

$$Ra = \sqrt{4(\delta_{D2} - \delta_{D1})^2 + (\delta_{P2} - \delta_{P1})^2 + (\delta_{H2} - \delta_{H1})^2} \quad (1)$$

The Hansen solubility parameters for a large number of solvents and polymers have already been determined and can be found in various reference sources.[30,31] In addition, the solubility parameters of most compounds can be estimated by group contribution theory, so long as group contributions are known for all groups present in the molecule.[30,31] This method involves the summation of the solubility parameters associated with each atom or group of atoms present in the molecule divided by the total molar volume of the molecule. In the work presented herein, group contribution theory is used to estimate the solubility parameters of 1,8-diiodooctane (DIO), $iI(TT)_2$, and $PC_{61}BM$. In the calculation for $PC_{61}BM$, the C_{60} unit is treated as one group with parameters previously reported by Hansen and Smith.[35] The calculated parameters for $iI(TT)_2$ and $PC_{61}BM$ are listed in **Table 1** with the details of the calculation shown in the SI. The solubility parameters of $iI(TT)_2$ and $PC_{61}BM$ are fairly similar with an *Ra* of 2.6 $MPa^{1/2}$. This relatively low *Ra* value indicates that the materials will not have a large thermodynamic driving force for phase separation. The family of solvents shown in Scheme 1 was selected such that all solvents have boiling points >200 °C at 760 Torr, with solubility parameters spanning a wide range as indicated in **Table 2**. The high boiling points are necessary to ensure that the SA remains in the film after the parent solvent has evaporated. It should be noted that the group contribution method is not an exact method for solubility parameter determination as it does not account for several aspects including π–π interactions, complementary hydrogen bonding groups, or donor and acceptor interactions between neighboring aromatic groups to name a few. The group contribution method is examined in this work for its use as a relatively rapid method to aid in SA selection.

The solubilities of $iI(TT)_2$ and $PC_{61}BM$ were measured in all of the solvents, including chlorobenzene (CB), by adding a sufficient amount of the material to the solvent such that after stirring overnight with a PTFE coated stir bar at room temperature a visible amount of precipitate could be observed by the naked eye. The stir bars were then removed and the solutions centrifuged at 3400 RPM for 45 min to separate non-dissolved material from the solution. Following centrifugation the supernatant was removed and known volumes of the supernatant were added to 3000 µL of chlorobenzene in a quartz cuvette. Absorbance measurements were taken at 3 to 5 different dilution values and the absorbance was compared to a previously measured calibration curve to determine the quantity of material dissolved in the original solution. The experimentally determined solubilities span over 4 orders of magnitude for both $iI(TT)_2$ and $PC_{61}BM$ in the various solvents as listed in Table 2.

The *Ra* values were calculated for $iI(TT)_2$ and $PC_{61}BM$ with all of the different solvents as listed in Table 2. The *Ra* values calculated for $iI(TT)_2$ correlate well with the measured solubilities, with the solubility and *Ra* showing a similar trend with the exception of PDMS and NMP. The fact that $iI(TT)_2$ shows a lower solubility in PDMS than would be predicted solely based on the *Ra* is expected given that PDMS is a polymer, and therefore according to the Flory-Huggins theory dissolution is less entropically favored as compared to the molecular solvents.[37,38] The higher solubility of $iI(TT)_2$ in NMP than the trend would predict is attributed to the presence of "NMP units" in the isoindigo core of the oligomer. The *Ra* values calculated for $PC_{61}BM$ with the various solvents show much more discrepancy with the measured solubilities than is observed for $iI(TT)_2$. This may partly be attributed to the unique electron accepting properties, the large area for π–π interactions, and/or the solvent dependent crystal structure of $PC_{61}BM$.[39]

2.2. Device Performance

We begin by presenting the device results, as these results provide the basis for the subsequent morphology, mobility, and V_{OC} discussions. Photovoltaic devices were fabricated through spin casting a 20 mg/mL solution of $iI(TT)_2$:$PC_{61}BM$ in chlorobenzene, with SA concentrations ranging from 0.1 to 1.0 mg/mL, onto PEDOT:PSS coated ITO followed by thermal annealing at 100 °C for 20 min. Device fabrication was completed by thermal deposition of 10 nm Ca and 100 nm Al. Devices were also made without thermal annealing for all SAs, and in all cases the thermally annealed devices displayed higher PCEs. The performance characteristics of the devices including the PCE, J_{SC}, fill factor (FF), and V_{OC} as a function of SA concentration are presented in **Figure 1** for all SAs applied. All data points represent an average of 6–8 cells on the same substrate, except for the no additive points that were determined from an average of over 60 individual cells.

For additive concentrations of 0.5 and 1.0 mg/mL the PCE either increases or remains constant for SAs where the solubility of both $iI(TT)_2$ and $PC_{61}BM$ are less than 0.8 mg/mL (poor solvents), and decreases for SAs where the solubility of

Table 2. Hansen solubility parameters for the applied SAs, calculated *Ra* values, and measured solubilities of $iI(TT)_2$ and $PC_{61}BM$ in the various solvents.

Solvent	Hansen Solubility Parameters[a]			*Ra*		$iI(TT)_2$ solubility [mg/mL]	$PC_{61}BM$ solubility [mg/mL]
	δ_D	δ_P	δ_H	$iI(TT)_2$	$PC_{61}BM$		
PDMS	16	0.1	4.7	11.7	9.6	0.002 ± 0.002	0.002 ± 0.002
TEG	16	12.5	18.6	20.3	20.4	0.012 ± 0.001	0.098 ± 0.004
HD	16.3	0	0	12.1	9.6	0.021 ± 0.001	0.20 ± 0.01
DEG-DBE	15.8	4.7	4.4	11.9	9.9	0.10 ± 0.01	0.75 ± 0.04
NMP	18	12.3	7.2	12.2	11.8	0.92 ± 0.07	37 ± 2
DIO	17.6[b]	4.8[b]	4.6[b]	8.4	6.6	2.3 ± 0.1	32 ±1
CB	19	4.3	2	6.2	4.0	15 ± 1	31 ± 1
CN	19.9[c]	4.9[c]	2.5[c]	4.7	3.0	27 ± 1	31 ± 1

[a]Measured values as reported by Hansen, all units are $MPa^{1/2}$;[30] [b]Calculated values using group contribution theory, group contribution values taken from Barton;[31] [c]Values from 2007 edition;[36] Molecular weight (MW) of PDMS is 2 000 g/mol.

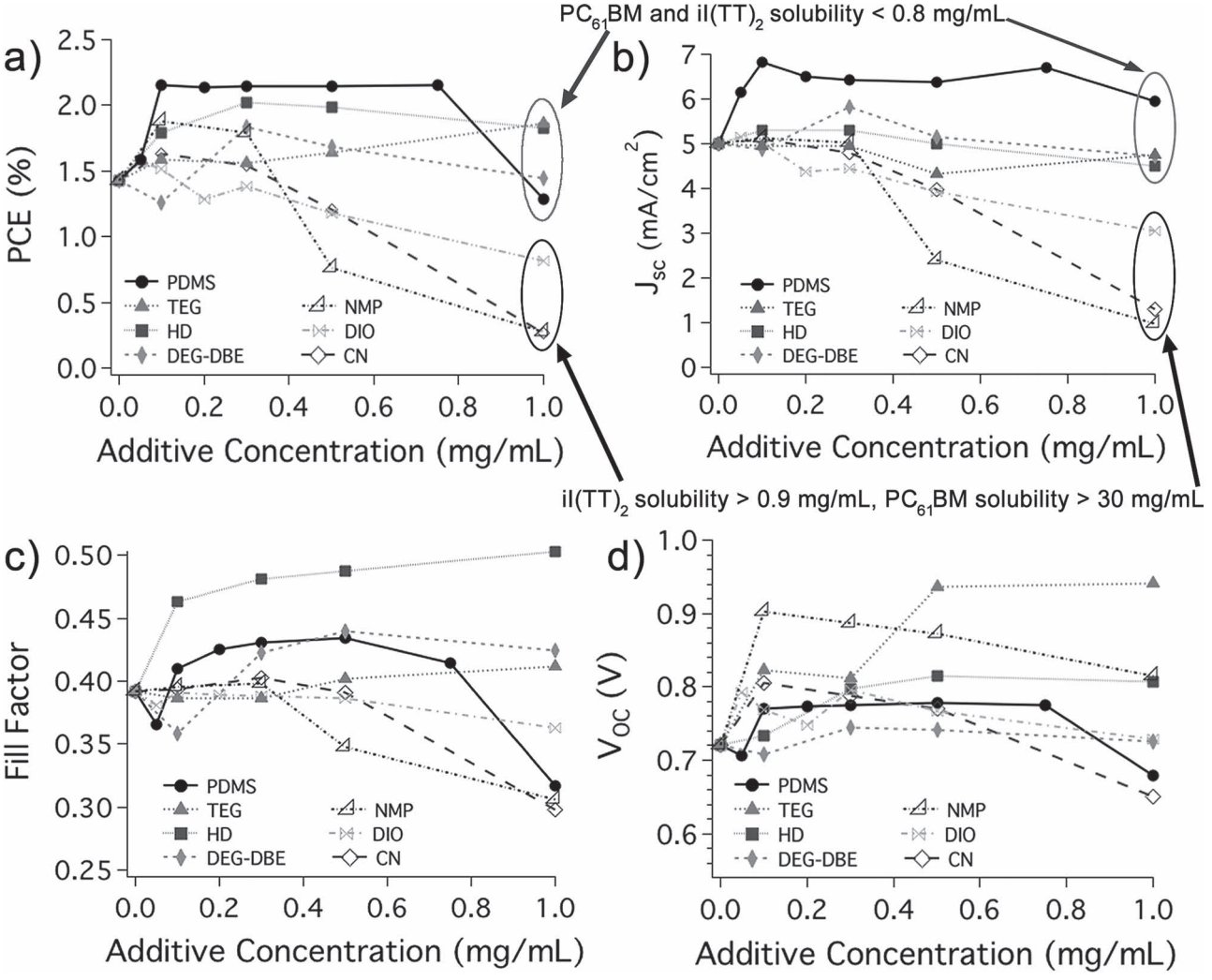

Figure 1. a) Power conversion efficiency, b) short circuit current density, c) fill factor, and d) open circuit voltage vs. additive concentration for $iI(TT)_2$:$PC_{61}BM$ cells after 100 °C thermal annealing.

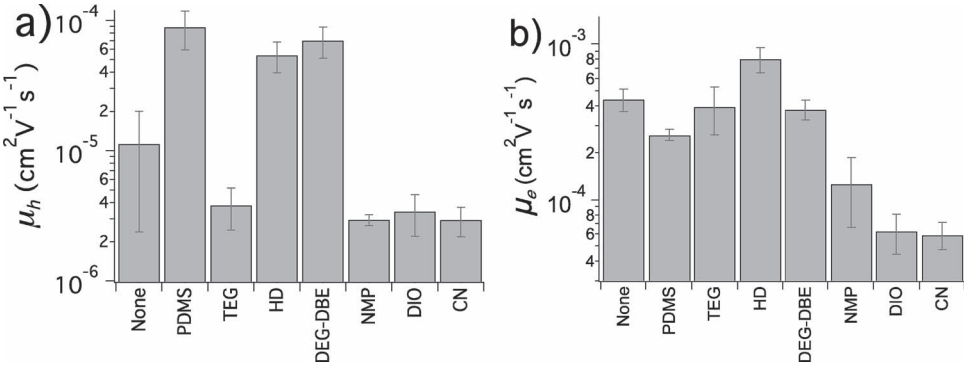

Figure 2. a) Hole and b) electron mobility values measured in iI(TT)$_2$:PC$_{61}$BM blends with 1.0 mg/mL of SA after thermal annealing.

iI(TT)$_2$ and PC$_{61}$BM are greater than 0.9 and 30 mg/mL (good solvents), respectively. The J_{SC} values show the same trend as observed for the PCE, again with PDMS showing the greatest J_{SC} improvement (PDMS MW is 14 000 g/mol unless otherwise noted). The fill factor shows an improvement from 0.39 to 0.49 with the use of HD as an additive, relatively minor improvements with the other three poor solvents (PDMS, TEG, and DEG-DBE), and decreased values with the three good solvents (DIO, NMP, and CN). An unexpectedly large increase in the V_{OC} from 0.72 V to 0.90 V is observed upon addition of 0.1 mg/mL NMP and an even greater enhancement to 0.95 V is observed upon addition of 0.5 or 1.0 mg/mL TEG. All other solvents show slightly enhanced V_{OC} values at lower concentrations, but are all within 0.1 V of the device with no additive. It should also be noted that significantly lower SA concentrations are used in these devices than is typically reported for polymer-based devices. These low concentrations were selected because they significantly affect device performance and morphology while also avoiding the wetting issues and poor PCEs that were realized with higher SA concentrations.

Without any thermal annealing, devices containing only 0.3 mg/mL of the various SAs show PCEs of ≈1.3% with the poor solvents PDMS, HD, or DEG-DBE as additives and PCEs <0.6% with no additive, TEG, NMP, DIO, or CN as shown in Supporting Information Figure 1. These results show a more significant influence of the SA prior to thermal annealing, indicating that they have a major influence on the morphology during film drying and may be incorporated to reduce the need for thermal annealing.[29]

Absorbance spectra of iI(TT)$_2$:PC$_{61}$BM blend films containing 1.0 mg/mL of each SA, as shown in Supporting Information Figure 2, display maxima between 596–601 nm due to the absorbance of the iI(TT)$_2$ oligomer.[40] Also apparent are peaks before and after the main peak at ca. 550 and 655 nm respectively. These peaks are attributed to either vibronic transitions or intermolecular transitions, both of which are correlated with the degree of intermolecular order.[41,42] A pure film of iI(TT)$_2$, which would be expected to display the highest degree of intermolecular ordering due to the absence of PC$_{61}$BM, displays a higher intensity peak at ca. 655 nm than any of the blend films with SAs both before and after thermal annealing. Assuming that the intensity and definition of the peak at ca. 655 nm is indicative of increased iI(TT)$_2$ ordering, than the absorbance data indicate that both before and after thermal annealing the films processed with the poor solvents show a lower degree of iI(TT)$_2$ ordering than those processed with the good solvents. This absorbance data suggests that the improved PCEs observed upon addition of the poor solvents both before and after thermal annealing are not attributed to increased intermolecular ordering.

The J_{SC} is primarily determined by the charge carrier mobilities and blend morphology when the absorbing materials and film thicknesses are kept constant. Therefore, the mobilities and morphology of the BHJ blends were investigated to probe the effects of the additive on the J_{SC}. Hole and electron mobilities were determined through space-charge limited current (SCLC) devices as detailed in the experimental section, with representative plots displayed in Supporting Information Figure 3 and 4. As shown in **Figure 2**, the hole mobilities (μ_h) are generally an order of magnitude lower than the electron mobilities (μ_e). The hole mobilities are shown to be between 5 and 9×10^{-5} cm^2 V^{-1} s^{-1} with the poor solvents PDMS, HD, and DEG-DBE as SAs. Interestingly, μ_h for films containing the good solvents DIO, NMP, and CN are over an order of magnitude lower at approximately 3×10^{-6} cm^2 V^{-1} s^{-1}. The film with no additive shows an intermediate hole mobility of 1.1×10^{-5} cm^2 V^{-1} s^{-1}; however, it should be noted that this film shows a significantly larger standard deviation than the other films. These μ_h values demonstrate that, with the exception of TEG, the poor solvents (i.e., iI(TT)$_2$ and PC$_{61}$BM solubility <0.8 mg/mL) improve hole mobility whereas the good solvents decrease the hole mobility. The electron mobilities are in the range of 5×10^{-5} to 8×10^{-4} cm^2 V^{-1} s^{-1}, which is comparable to other BHJ OPVs with PCBM as the electron acceptor.[8,20] Similar to the trend in μ_h, μ_e is lower for the good solvents and higher for the poor solvents. With the electron mobilities exceeding the hole mobilities for all SAs, it is expected that the influence of the SA on μ_h will be a more dominant factor in determining device performance relative to μ_e.

2.3 Film Morphologies

To gain a relatively complete picture of film morphologies in the iI(TT)$_2$:PC$_{61}$BM blends with various SAs, complementary techniques consisting of atomic force microscopy (AFM), top-down

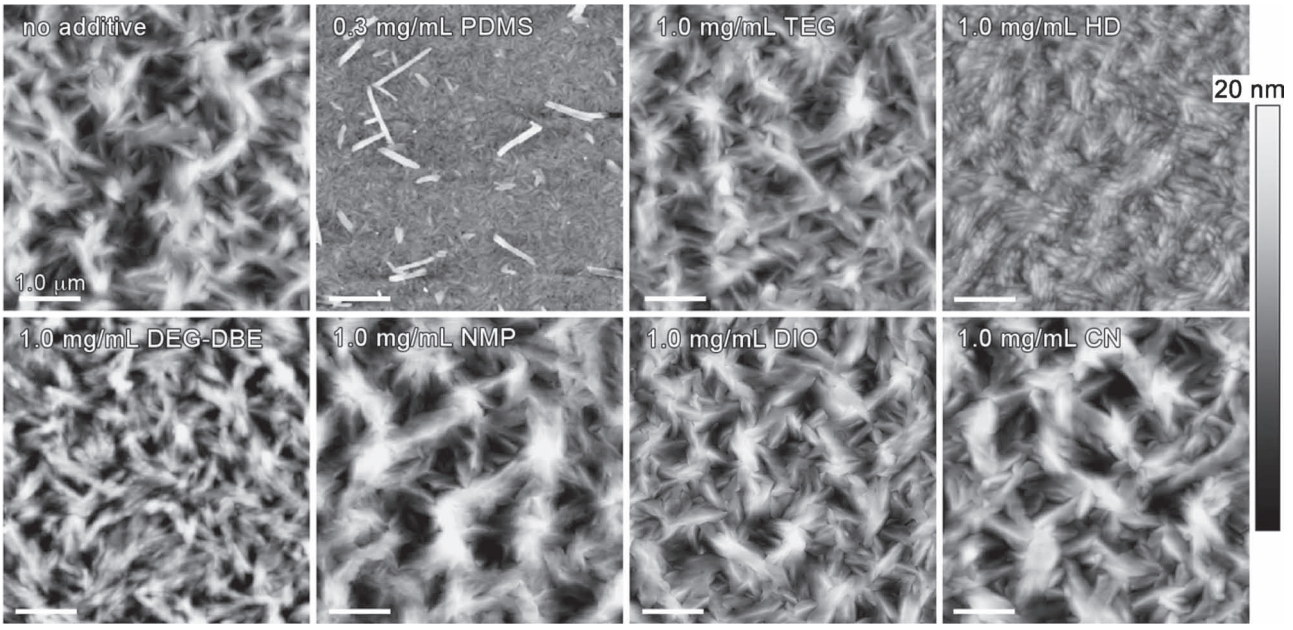

Figure 3. AFM height images of $iI(TT)_2$:$PC_{61}BM$ cells with additives after 100 °C thermal annealing.

transmission electron microscopy (TEM), cross-sectional TEM, and X-ray photoelectron spectroscopy (XPS) were utilized. AFM height imaging provides an effective means of imaging the morphology at the top surface of the film; however, it provides little to no information about the bulk morphology or the surface composition. Therefore, top-down and cross-sectional TEM are utilized to help generate a more complete picture by probing the morphology in the bulk. Additionally, XPS is used to gain information about the elemental composition at the film surface.

The AFM height images presented in **Figure 3** show large features when no additive is applied and a significantly reduced feature sizes upon the addition of 0.3 mg/mL PDMS. Note that only 0.3 mg/mL PDMS was used as compared to 1.0 mg/mL of the other SAs due to the accumulation of PDMS at the top surface which made AFM imaging difficult at high concentrations. The feature sizes for the films containing 1.0 mg/mL of the poor solvents HD and DEG-DBE are larger than the device with 0.3 mg/mL PDMS, but still smaller than the film with no additive. The trend among these three SAs is that the feature size increases as the solubilities of $iI(TT)_2$ and $PC_{61}BM$ in the SA increase. The good solvents NMP, DIO and CN all show similar or increased feature sizes as compared to the film with no additive, with the 1.0 mg/mL NMP film displaying the largest features. An exception to the solubility trend of increasing feature sizes with increased solubility is that of TEG, which shows a surface morphology nearly identical to that of the film with no additive. This is attributed to the fact that TEG has a high tendency for H-bonding, which likely results in TEG accumulation at the PEDOT:PSS interface and, thereby, little effect is observed on the top surface morphology.

Top-down bright field TEM images of the films with 1.0 mg/mL of each additive show generally increasing domain sizes as the solubility of the materials in the SAs increase as shown in **Figure 4**. The films with TEG and no additive show similar morphologies, with both larger and smaller domains present. The similarity between these two film morphologies is consistent with localization of TEG at the PEDOT:PSS interface. The film with PDMS shows significantly more uniform domain sizes in the same range as the device with no additive. The largest domain sizes are observed for the NMP containing film, which may be expected given the high solubility of $PC_{61}BM$ and the large difference in solubility between $iI(TT)_2$ and $PC_{61}BM$ in NMP (Table 2). In all films the domain sizes observed in the TEM images are significantly smaller than the feature sizes observed in the AFM images. This suggests that the surface morphologies differ significantly from those present in the bulk. These differing morphologies highlight the importance of using TEM and AFM as complimentary characterization tools, rather than making an incorrect assumption that the surface morphology imaged through AFM is representative of the bulk.

The interplay between domain size, hole mobility, and short circuit current is highlighted by comparing the three variables as presented in Figure 4. That is, roughly speaking the J_{SC} varies inversely with the domain size, i.e., domain size decreases and J_{SC} increases, and directly with the limiting charge-carrier mobility, which in this case is the hole mobility. For example, the device with no additive and the device with TEG show similar domain sizes, hole mobilities, and J_{SC} values (note that μ_h and J_{SC} values are presented in Figure 4). The device with PDMS shows similar domain sizes as the no additive device with an order of magnitude higher μ_h, thereby the device with PDMS has a higher J_{SC}. Moreover, the devices with HD and DEG-DBE show increased domain sizes relative to the device with no additive, yet they show similar J_{SC} values due to the higher hole mobilities. Furthermore, the devices processed with the good solvents show larger domain sizes than the device with no additive and lower hole mobilities, thereby resulting in reduced J_{SC} values.

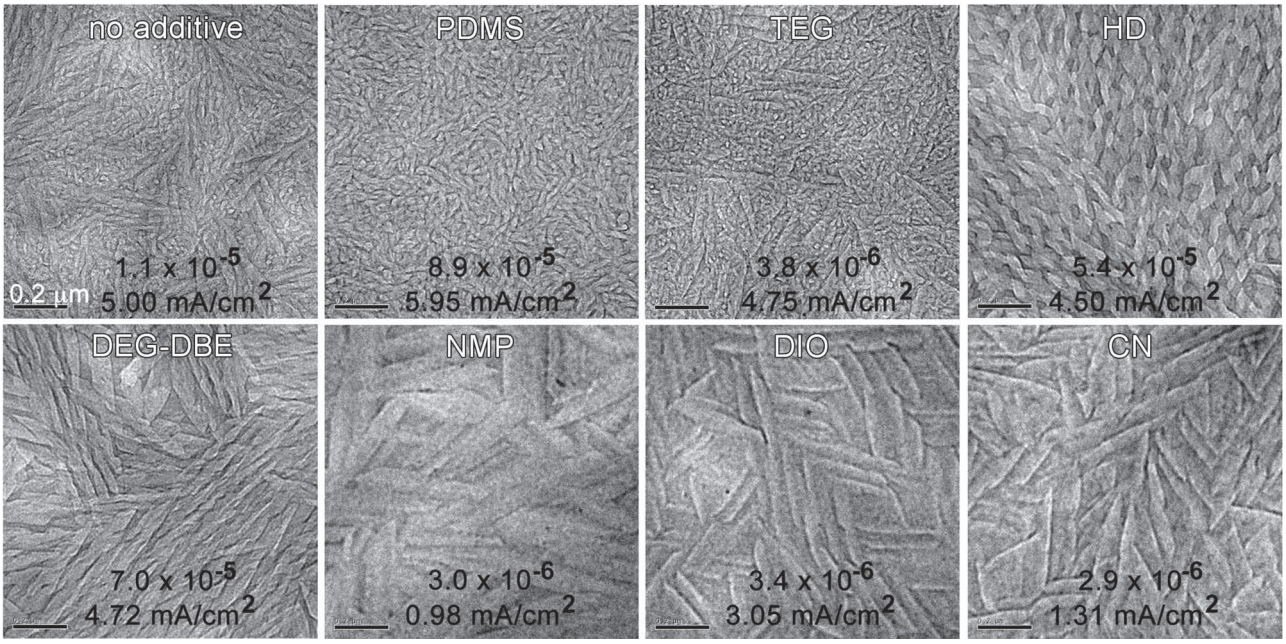

Figure 4. Top down bright field TEM images of $iI(TT)_2$:$PC_{61}BM$ cells with 1.0 mg/mL SA after 100 °C thermal annealing, with μ_h ($cm^2\ V^{-1}\ s^{-1}$) and J_{SC} values indicated at the bottom of each image. The darker regions are $PC_{61}BM$ rich while the lighter regions are $iI(TT)_2$ rich as shown in Figure 5.

The trend in domain size may be explained by the stronger interactions of the components with the better solvents leading to increased time for domain growth, thereby resulting in larger domains. Based on this explanation, it may be predicted that the increased organizational time would lead to higher mobilities. This is not observed and it is possible that the more favorable material-solvent interactions lead to less pure D and A domains (i.e. more D present in A phase and vice versa), or small isolated A domains in D and vice versa which act as charge traps. The more unfavorable interactions with the poor solvents would cause nucleation/aggregation to occur earlier in the film drying process than the good solvents, thus potentially leading to more pure D and A phases, smaller domains due to the presence of more nucleation sites, and/or a decreased number of isolated domains. The more weakly interacting solvents would also introduce more degrees of freedom into the drying film than the film without any additive, which would allow more time for molecular organization.

Enhanced aggregation during film drying has previously been suggested to explain the larger domain sizes and enhanced crystallinity of P3HT:$PC_{61}BM$ and PCPDTBT:$PC_{71}BM$ cells upon addition of 1,8-octanedithiol or DIO.[20,43] In these previous reports, the SA is a good solvent for the fullerene derivative, which is in contrast to our work where the best performing SAs are poor or non-solvents for both $iI(TT)_2$ and the fullerene. The smaller amount of additives required in this work as compared to previous examples in polymer based BHJ OPVs may be attributed to the fact that this is a molecular system whereby molecular diffusion (or the molecular mobility term in the modified Cahn-Hilliard equation) would be higher.[44–45] As such, film organization can occur much more easily and rapidly during film drying as compared to the more restrictive polymeric systems, thereby the SA effects on morphology are more apparent at lower additive concentrations.

It is also possible that the specific parts of the molecules that interact more strongly with the SAs may be a factor in determining mobilities. For example, the poor solvents all have stronger interactions with the alkyl side-chains, whereas the good solvents are generally expected to have stronger interactions with the conjugated cores. These mechanistic explanations are likely contributing factors to the resulting morphology and device performance; however, as with other SAs more experimental and theoretical work is necessary to develop a complete mechanistic understanding.

Cross sections of selected devices that display outstanding trends were prepared with the use of a focused ion beam (FIB) and imaged through TEM as displayed in **Figure 5**. A film consisting of a pure $PC_{61}BM$ layer and a pure $iI(TT)_2$ layer separated by an aluminum interlayer, as shown in Figure 5e, shows no evidence of beam damage and allows identification of the darker phase as $PC_{61}BM$ and the lighter phase as $iI(TT)_2$. Figure 5a shows the device with no additive and also denotes the layered structure of ITO/PEDOT:PSS/$iI(TT)_2$:$PC_{61}BM$/Ca/Al. In this device with no additive large domains near the top surface of the active layer and smaller domains near its bottom surface are observed, which corresponds well with the large and small domains observed in the top down TEM images. It is also evident in Figure 5a that the device shows the opposite vertical phase separation as desired, with the device appearing more $iI(TT)_2$ rich (lighter in color) near the electron collecting Ca/Al electrode. Conversely, the device with 0.5 mg/mL HD shows evidence of more favorable vertical phase separation with a dark, $PC_{61}BM$ rich band appearing near the Ca/Al electrode. Although, above this dark band is a thin light $iI(TT)_2$ rich band. Given the similar mobilities observed in the PDMS, HD, and DEG-DBE containing devices, the enhanced FF (Figure 1c) observed in the HD containing device may potentially be

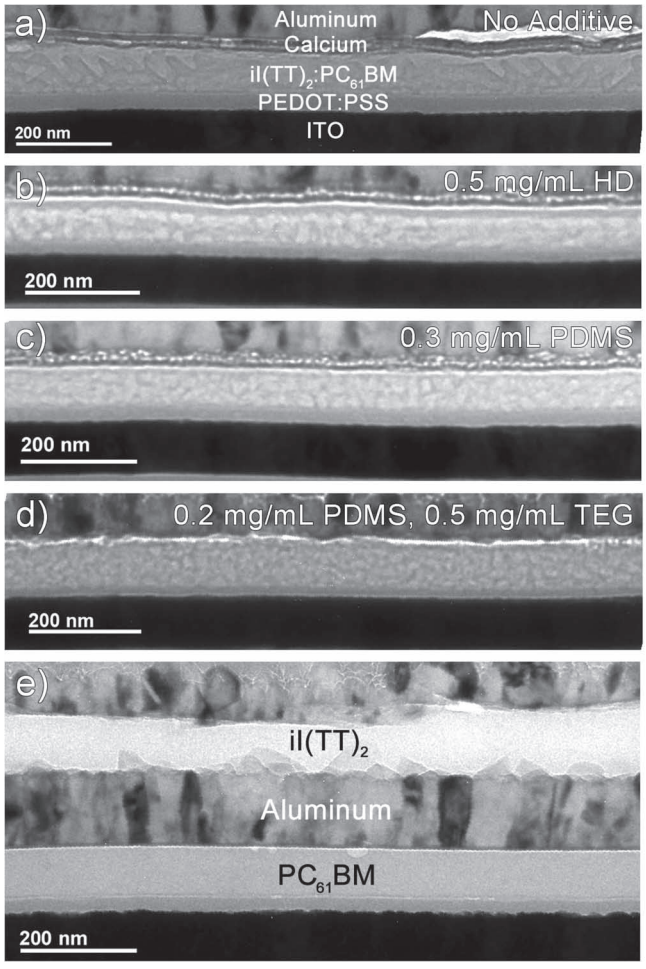

Figure 5. Cross-sectional bright field TEM images of iI(TT)$_2$:PC$_{61}$BM cells with a) no additive, b) 0.5 mg/mL HD, c) 0.3 mg/mL PDMS, d) 0.2 mg/mL PDMS and 0.5 mg/mL TEG, and e) control bilayer film showing a layered structure consisting of ITO/PEDOT:PSS/PC$_{61}$BM/Al/iI(TT)$_2$/Al after 100 °C thermal annealing.

attributed to this favorable vertical phase separation. The 0.3 mg/mL containing PDMS device shown in Figure 5c shows a more uniform morphology throughout the active layer than the device with no additive and consistent domain sizes on the order of ≈10–25 nm. Additionally, only minimal signs of vertical phase separation are observed. Devices containing either 0.1 mg/mL NMP or 0.5 mg/mL TEG were also imaged to probe for any vertical phase separation which may be contributing to the enhanced V_{OC}. No vertical phase separation was observed as can be seen in Supporting Information Figure 5. As will be addressed later, a device consisting of both 0.2 mg/mL PDMS and 0.5 mg/mL TEG was also fabricated with a solution concentration of 25 mg/mL. This device shows a uniform morphology similar to the device with only 0.3 mg/mL PDMS, but with slightly smaller domain sizes and a slightly thicker active layer as presented in Figure 5d.

The chemical composition of the top surface of the blend films was probed for films without any SA, with PDMS, and with HD. These films were made in an identical manner to the devices, only no top Ca/Al electrodes were deposited. XPS measurements are presented with an electron take off angle of 45°, which primarily probes the first ca. 5 nm of the films based on previously reported attenuation lengths.[46–48] The results presented in **Table 3** indicate the top surface is composed of ≈90 to 100% iI(TT)$_2$ in all films, which is contrary to the ideal morphology where the top surface would be PC$_{61}$BM enriched. Additionally, the device with HD also has a iI(TT)$_2$ surface composition of 100 ± 10%. This indicates that the PC$_{61}$BM enriched layer observed in the cross-section TEM image must lie beneath an initial ca. 5 nm of iI(TT)$_2$. The fact that the devices all show significantly enhanced iI(TT)$_2$ surface compositions, yet device performance is still relatively high is in agreement with work presented by the Kahn and Loo groups.[49] In their study it was demonstrated that P3HT:PC$_{61}$BM cells show minimal variation between devices where the relative PC$_{61}$BM composition is 3% or 35–45% at the electron collecting contact.

Recently it has been reported by Yamakawa et al. that a block PMMA-PDMS polymer can enhance the performance of BHJ OPVs by forming a PDMS rich buffer layer at the cathode, which they mention may suppress charge recombination.[50,51] With these results in mind, the effect of PDMS as a potential buffer layer was examined by probing the surface composition of a PDMS containing blend film and exploring the use of PDMS with lower molecular weight (MW) that evaporates from the film during drying. As shown in Table 3 for a device containing 0.2 mg/mL PDMS of 14 000 g/mol MW, the surface composition to a depth of ca. 5 nm consists of ≈22% PDMS, where as the total concentration of PDMS relative to iI(TT)$_2$ and PC$_{61}$BM is only 1% by weight. The percent composition of iI(TT)$_2$, PC$_{61}$BM, and PDMS were calculated based on the elemental composition and the known chemical formulas as shown in Supporting Information Table 4 and Supporting Information Equation 5–7. Additionally, electron take off angle dependent XPS measurements as presented in Supporting Inforomation Table 5 and Figure 6 were performed and confirm

Table 3. XPS elemental analysis of film surface.

Additive	C[a)] [%]	N[a)] [%]	O[a)] [%]	S[a)] [%]	Si[a)] [%]	iI(TT)$_2$[b)] [%]	PC$_{61}$BM[b)] [%]	PDMS[c)] [%]
none	88.4	2.7	3.7	5.3	0	91	9	0
Hexadecane	87.5	3.1	3	6.4	0	100	0	0
PDMS (14 000 g/mol)	76.8	1.6	11.9	4.1	5.6	62	10	22
PDMS (410 g/mol)	88.7	2.8	3.6	4.8	0	88	12	0

[a)]Errors in elemental composition are approximately ±0.5%, resulting in errors in; [b)]percent iI(TT)$_2$ and PCBM composition of ±10% and errors in; [c)]percent PDMS composition of ±2%.

that PDMS is localized on the surface. These angle dependent measurements indicate a PDMS composition of 58% at a take off angle of 15°, whereby the probing depth would be shortest, and a PDMS composition of 18% at a take off angle of 90°, whereby the probing depth would be greatest. These results support the previous report that PDMS vertically phase separates to the top surface of the film.[50]

To test if this buffer layer results in the device improvement, lower MW PDMS was used as an additive. For the device containing 0.2 mg/mL of 410 g/mol MW PDMS no Si was observed upon XPS analysis, indicating that the low MW PDMS evaporates during film drying. Although the 410 g/mol MW PDMS evaporates, a PCE enhancement from 1.42% with no PDMS to 2.35% with this low MW PDMS occurs, which is similar to the 2.30% observed with 14 000 g/mol PDMS as shown in Supporting Information Figure 7. Therefore, it can be concluded that for these devices the PCE increase upon PDMS addition is due to the morphology and increased hole mobility and not the formation of a buffer layer.

It should be noted that devices were made with PDMS samples ranging in molecular weight from 237 to 117 000 g/mol. With the exception of the 237 g/mol MW PDMS sample, which has too low of a boiling point (152–153°C) to serve as an effective additive, the PCE of devices with 0.2 mg/mL PDMS are consistently between 2.17 and 2.55% throughout the MW range tested. Correspondingly, the morphologies as imaged with AFM are similar for PDMS MWs ranging from 770 to 117 000 g/mol as shown in Supporting Information Figure 8. This also indicates that if residual PDMS is found to negatively affect device stability, the problem could be avoided while maintaining the same performance enhancement by using lower MW PDMS as an additive.

2.4. Interfacial Effects and Mixed Additives

Quite unexpectedly, both NMP and TEG were found to significantly increase the V_{OC}. With their high hydrogen bonding parameters and current knowledge of the V_{OC} it was hypothesized that the origin of the increase was due to an alteration in the energetics of the PEDOT:PSS/BHJ interface resulting from an accumulation of the SAs at the interface. If this assumption was correct then NMP or TEG could be combined with a second SA designed to increase the J_{SC}, thereby resulting in both an elevated V_{OC} and J_{SC}. Since TEG yielded the highest V_{OC} and PDMS the highest J_{SC}, these two SAs were both added to the active layer processing solution at 0.5 and 0.2 mg/mL respectively. The combination of these two additives resulted in a device with a J_{SC} of 7.0 mA/cm^2, V_{OC} of 0.93 V, FF of 0.47, and PCE of 3.06 ± 0.14%. Compared to the device with no additive this is a 40% increase in the J_{SC}, which is approximately the same as with only PDMS as a SA, a 29% increase in the V_{OC} which is the same as with only TEG as a SA, and a 21% increase in the FF which is 10% higher than with only PDMS or only TEG, resulting in a 115% increase in the PCE. The fact that these two additives combined produce nearly the same improvements as each does independently supports that the TEG is acting on the PEDOT:PSS interface while PDMS improves the film morphology.

To further test this hypothesis the effect of spin coating a layer of TEG onto the PEDOT:PSS surface prior to active layer deposition was examined. In this device a 1 mg/mL TEG in chlorobenzene solution was spun cast onto the PEDOT:PSS layer and allowed to dry for 20 min. The iI(TT)$_2$:PC$_{61}$BM active layer containing 0.2 mg/mL PDMS and no TEG was subsequently spun cast and thermally annealed. As shown in Figure 6a, the V_{OC} of the device with the 1.0 mg/mL TEG prespin is slightly lower than the device with 0.5 mg/mL TEG in solution, 0.88 ± 0.01 V vs. 0.93 ± 0.01 V, but 0.11 V higher than the device with only 0.2 mg/mL PDMS and no TEG. This supports that the enhancement in the V_{OC} is attributed to modification of the PEDOT:PSS/BHJ interface by TEG.

Previously it has been demonstrated that the work function of PEDOT:PSS is sensitive to the PEDOT to PSS ratio at the surface,[52,53] thermal annealing conditions,[54] UV treatment,[55] exposure to water vapor,[54] pH of the casting solution,[56] acid or base exposure,[57] and the addition of dopant solvents such as glycerol or sorbitol.[58,59] Considering this sensitivity, it is likely that the addition of the strongly H-bonding TEG results in a modified PEDOT:PSS work function. This would likely have little effect in P3HT:PC$_{61}$BM cells where near ohmic contact occurs at the PEDOT:PSS/P3HT interface; however, in this system where the HOMO is ≈0.5 eV below the work function of PEDOT:PSS an increase in work function would likely result in a higher V_{OC}. This is supported by previous work that shows an increasing V_{OC} until the cathode and anode work function difference reaches a large enough value beyond which the V_{OC} saturates.[60,61]

The device was further optimized to reach a PCE of 3.31 ± 0.15% with a J_{SC} of 7.8 mA/cm^2, V_{OC} of 0.95 V, and FF of 0.45 through increasing the iI(TT)$_2$:PC$_{61}$BM solution concentration to 25 mg/mL with 0.2 mg/mL PDMS and 0.5 mg/mL TEG, as shown by the *J*–*V* curve in **Figure 6**b. The cross-section TEM image of this device is presented in Figure 5d and shows a similar morphology to the device containing only PDMS, but with a thicker active layer and slightly decreased domain sizes as previously mentioned. This optimized device was compared with an identical device fabricated with 5 nm MoO_3 in place of PEDOT:PSS and only 0.2 mg/mL PDMS in solution (no TEG). This comparison was made since MoO_3 is known to have a large work function and form good ohmic contact with deep HOMO level materials. The device with MoO_3 shows a nearly identical V_{OC} as the device with 0.5 mg/mL TEG as displayed in Figure 6b. Additionally, the device with MoO_3 shows a slightly decreased J_{SC} of 7.1 mA/cm^2 with an increased FF of 0.54, resulting in a PCE of 3.67 ± 0.12%. To confirm these results, this device gave a PCE of 3.70 ± 0.11% when tested outside under full sun (95 mW/cm^2) in Gainesville, FL at 2:00 pm on May 2, 2011.

To further probe the possible origin of the increased V_{OC} and increased device performance upon the use of TEG and PDMS as SAs and upon substitution of PEDOT:PSS with MoO_3, electroabsorption measurements were performed. This technique measures the changes in optical constants of materials under applied electric fields and can be used to probe the electric fields within organic electronic devices.[62–65] Equations 7 and 8 in the Supporting Information along with the plots shown in Supporting Information Figure 9 were used to extract the built-in voltage (V_{BI}) from the electroabsorption data. Devices were fabricated with LiF(1nm)/Al(100nm) cathodes in place of the

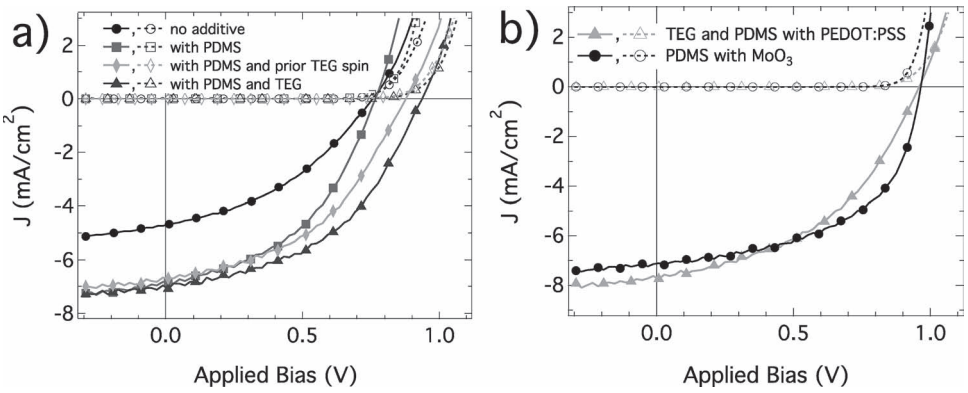

Figure 6. Representative current density vs. voltage characteristics under simulated AM1.5 illumination (solid lines) and in the dark (dashed lines) of iI(TT)$_2$:PC$_{61}$BM devices a) processed at 20 mg/mL on PEDOT:PSS and b) processed at 25 mg/mL on PEDOT:PSS and MoO_3 with and without PDMS and TEG as additives.

normally used Ca(10nm)/Al(100nm) cathodes, see Supporting Information Table 6 for device results, to enhance device stability outside of the glovebox, which likely decreases V_{BI} slightly. From the electroabsorption data, the V_{BI} was determined to be 1.06 ± 0.01 V and 1.13 ± 0.01 V for the device with 0.2 mg/mL PDMS and the device with both 0.2 mg/mL PDMS and 0.5 mg/mL TEG on PEDOT:PSS respectively. This increase in the V_{BI} along with the previous data supports that the addition of TEG results in a modification of the electronic properties of the PEDOT:PSS/BHJ interface. The increase of the V_{OC} by ≈0.2 V upon addition of TEG is larger than would be expected from the V_{BI} increase of 0.07 V alone. This larger than expected V_{OC} increase indicates that the effect of TEG on the PEDOT:PSS/BHJ interface is likely more complicated than a simple increase in the work function of PEDOT:PSS.

A further increase in the V_{BI} to 1.28 ± 0.01 V is observed for the device with 0.2 mg/mL PDMS as a SA on MoO_3. This increase in the V_{BI} is expected due to the higher work function (5.4–6.0 eV) of MoO_3 as compared to PEDOT:PSS.[66] As a consequence of the higher V_{BI}, the driving force for charge extraction is enhanced resulting in decreased recombination and a higher FF. The fact that MoO_3 and the use of TEG as an additive result in the same V_{OC} suggests that the limit of the V_{OC} for this particular BHJ blend is reached at 0.95 V.

3. Conclusions

It has been demonstrated that Hansen solubility parameters calculated using group contribution theory can serve as an effective method for predicting material solubilities in various solvents and guiding selection of an appropriate SA. For the thiophene/isoindigo-based molecular system investigated, it was observed that device performance generally increased when a poor solvent (i.e., iI(TT)$_2$ and PC$_{61}$BM solubility <0.8 mg/mL) was employed and decreased when a better solvent (i.e., iI(TT)$_2$ and PC$_{61}$BM solubility >0.9 and >30 mg/mL respectively) was used. Additionally, the hole mobilities increased upon application of the poor solvents PDMS, HD, and DEG-DBE as additives, and decreased with the use of the good solvents NMP, DIO, and CN as additives. The electron mobilities remained nearly constant or increased slightly upon addition of a poor solvent, and decreased by an order of magnitude upon addition of a good solvent. The D and A domains were shown to increase in size as the solubility of iI(TT)$_2$ and PC$_{61}$BM in the SA increased. A strong correlation was observed between mobility, domain size, and J_{SC}, with PDMS displaying small domains, high mobilities, and therefore the highest J_{SC}. Application of varying molecular weights of PDMS combined with XPS analysis revealed that the improvement upon application of PDMS is not due to the formation of a PDMS buffer layer. SAs with high hydrogen bonding parameters including NMP and TEG were shown to increase the V_{OC} by ≈0.2 V. This V_{OC} enhancement is attributed to the effect of the additives on the PEDOT:PSS/active layer interface. By combining the complementary additives PDMS and TEG a PCE of 3.31 ± 0.15% was obtained; similarly, the use of PDMS as an additive in a device with MoO_3 in place of PEDOT:PSS resulted in a further increased PCE of 3.67 ± 0.12%. The increase in V_{OC}, FF, and PCE is partly attributed to the higher V_{BI} present in the device with TEG as an SA, with the further increase in PCE upon substitution of MoO_3 for PEDOT:PSS being attributed to a higher V_{BI}. In summary, it has been demonstrated that SAs may be chosen in a predictable manner and effectively used to tune the morphology and interfaces in molecular BHJ OPV devices resulting in significant enhancements in PCE.

4. Experimental Section

The synthesis of iI(TT)$_2$ is as previously reported.[40] PC$_{61}$BM was purchased from SES Research, 99% purity, and used as received. Additionally, PC$_{61}$BM was also purchased from nano-C, 99.5% purity, for a comparison in solubility measurements. All molecular weights of polydimethylsiloxane (PDMS) are end capped with trimethylsiloxane, were purchased from Alfa Aesar, and used as received. Triethylene glycol (TEG), 1-methyl-2-pyrrolidinone (NMP), and chlorobenzene (CB) were purchased anhydrous from Sigma Aldrich and deoxygenated through freeze-pump-thawing before use. Diethylene glycol dibutyl ether (DEG-DBE) was purchased from Alfa Aesar, distilled over CaH to remove water, and deoxygenated through freeze-pump-thawing. Hexadecane

(HD), 1-chloronaphthalene (CN), and 1,8-diiodoctane (DIO) were purchased from Sigma Aldrich and used as received. It should be noted that the SAs which were anhydrous and degassed were those known to uptake more water and oxygen.

The solubilities of iI(TT)$_2$ and PC$_{61}$BM were determined at room temperature (21–24 °C) following the procedure described in the text. Absorbance measurements were acquired with a PerkinElmer Lambda 25 UV-Vis spectrometer and absorbance at peak wavelengths, 330 and 432 nm for PC$_{61}$BM and 359 and 587 nm for iI(TT)$_2$, were used in determining the solution concentrations. The 2 000 g/mol MW PDMS was used as this had a lower viscosity than the 14 000 g/mol MW PDMS and thus allowed for better removal of undissolved PC$_{61}$BM clusters from solution. Dissolution by sonication followed by stirring overnight was also performed for selected solvents (CN, CB and DIO), with nearly identical solubility values as obtained for the solutions stirred overnight without prior sonication. It should also be noted that the solubility of PC$_{61}$BM in 1-chloronaphthalene was performed on 3 separate occasions utilizing PC$_{61}$BM purchased from two different companies, SES Research and nano-C, with nearly identical results. To verify that soluble PC$_{61}$BM was not being removed through centrifugation, the solubility was also measured using a similar procedure as reported by Walker et al.[17] Following this procedure, the PC$_{61}$BM in chloronaphthalene solution was stirred for 2 days followed by sitting in the dark without stirring for 3 days to allow for insoluble material to precipitate out. The soluble fraction was collected, filtered with a 0.2 μm PTFE filter, diluted with chlorobenzene, and absorbance measurements recorded. This method yielded the same solubility as the centrifugation method.

Devices were fabricated on 25 mm × 25 mm prepatterned ITO coated glass substrates (sheet resistance = 15 ohms/square.) with a layered structure of glass/ITO/PEDOT:PSS/iI(TT)$_2$:PC$_{61}$BM/Ca/Al, with 5 nm MoO_3 substitued in place of PEDOT:PSS where indicated. The ITO substrates were cleaned through sequential sonication in sodium dodecyl sulfate solution, deionized (18 MΩ) water, acetone and isopropanol for 15 min each. Substrate cleaning was completed through exposure to an oxygen plasma for 20 min followed immediately by spin coating with PEDOT:PSS (Clevios P VP AI4083) at 5000 RPM in the ambient atmosphere. PEDOT:PSS was annealed in an argon filled glovebox with H_2O and O_2 typically <0.1 ppm on a hotplate at 130 °C for 20 min. Solutions of iI(TT)$_2$ and PC$_{61}$BM were prepared at 20 mg/mL unless otherwise noted and stirred overnight. The solutions were then heated to 60 °C with stirring for at least 1 h before combining to form a 1:1 (by weight) solution. Solutions containing 10 mg/mL of the particular SA in chlorobenzene were then added to the iI(TT)$_2$:PC$_{61}$BM blend solutions to reach the appropriate additive concentration, and the solution stirred at 60 °C for at least 30 min prior to spin coating. Solutions were filtered with a 0.45 μm PTFE filter coupled with a cleaned glass syringe (cleaned through sequential sonication in methanol, chloroform, toluene, and isopropanol for 15 min each) directly onto the substrate followed by spin coating at 1000 RPM for 60 s with a 3 s ramp. Unless otherwise noted, the films were annealed at 100 °C on a hotplate in the Ar glovebox for 20 min prior to thermal vapor deposition of 10 nm of Ca and 100 nm of Al at a pressure of 1×10^{-6} mbar. Current-voltage characteristics were collected in the glovebox with a Keithley 2400 sourcemeter. Cells were illuminated with 100 mW/cm^2 simulated AM1.5 illumination produced from a Xe arc lamp fitted with an AM1.5 filter. All devices featured 8 independently addressable cells with areas of 0.071 cm^2 per cell, of which the average performances are reported along with the standard deviations.

For the electron mobilities LiF/Al was used as the electron-injecting electrode with Al as the electron-collecting electrode. For hole mobilities the BHJ layer was sandwiched between MoO_3 on ITO as the hole-injecting electrode and Au as the hole-collecting electrode. MoO_3 was used in place of PEDOT:PSS as it has previously been shown to yield better hole injection for higher HOMO materials.[67] As an exception, hole mobility measurements for the TEG containing film were performed with PEDOT:PSS in place of MoO_3, as for TEG only PEDOT:PSS resulted in better hole injection than MoO_3. The mobilities were extracted by fitting the *J–V* characteristics in the SCLC regime with the field dependent SCLC equation as shown in Supporting Information Figure 2,3 and Supporting Information Equation 4.[68–70] Devices were prepared on ITO coated substrates that were cleaned as previously detailed and transferred to the thermal vapor deposition chamber immediately following oxygen plasma exposure. Approximately 5 nm of MoO_3 (Sigma Aldrich, 99.99% purity) was then deposited onto the ITO coated substrates or 100 nm Al (Alfa Aesar 99.99% purity) on glass substrates via thermal vapor deposition at a pressure of 2 to 4×10^{-6} mbar. The active layer solutions were prepared, spun cast onto the MoO_3/ITO or Al coated glass substrates, and annealed at 100 °C following the above described procedure. Thermal deposition of the bottom electrodes and all procedures thereafter were performed in the Ar filled glovebox, with solutions spun cast immediately upon removal of substrates from the evaporator to limit the shift in the energy levels of MoO_3.[66] The devices were completed by thermal vapor deposition of a 70 nm thick gold electrode (hole mobility) or an LiF(1nm)/Al(100nm) electrode (electron mobility) and the current voltage characteristics were collected in the Ar glovebox with a Keithley 2400 sourcemeter. All devices consisted of 8 individually addressable 3 mm diameter pixels. Data was fit using the field dependent SCLC equation as displayed in the Supporting Information. All reported values are averages of 6–8 pixels with error bars as ± 1 standard deviation.

AFM images were acquired with the use of a Veeco Innova scanning probe microscope in tapping mode using MikroMasch NSC15 tips with a resonant frequency ≈325 kHz and a force constant ≈40 N/m. Multiple AFM images were taken of each device with all images taken within 2 mm of a cell. Samples for top-down TEM analysis were prepared by floating the iI(TT)$_2$:PC$_{61}$BM blend off of the PEDOT:PSS layer in deionized water and collecting on a carbon coated TEM grid. The cross-section samples were fabricated from the actual solar cell area following our previously reported procedure.[71] All samples were imaged with a JEOL 200CX TEM in bright field mode with an accelerating voltage of 200 kV.

XPS measurements were performed with a Perkin Elmer 5100 XPS system with a Mg Kα X-ray source (1253 eV) and a hemispherical electron energy analyzer. The substrate was angled 45° relative to the detector entrance unless reported otherwise. For angle dependent measurements the angle between the substrate and detector entrance was varied from 15 to 90°. Scans were performed with data being collected in 0.1 eV increments with a collection time of 50 ms at each increment and pass energy of 35.75 eV, 10 scans were averaged for each spectra. Atomic ratios were calculated using the AugerScan XPS analysis software that automatically adjusted for the previously calibrated elemental sensitivity.

The devices for electroabsorption were made in an identical manner as described above, except a LiF(1nm)/Al(100nm) cathode was used in place of Ca(10nm)/Al(100nm). Additionally the devices were encapsulated using UV-curable epoxy and a piece of microscope cover glass. The use of LiF/Al and encapsulation was necessary as the devices were exposed to air for several days as they were taken from Gainesville, FL to Washington, DC for testing. In our experimental setup for electroabsorption measurements, light from a quartz halogen source is fed into a monochromator from Acton research and then focused onto the pixel of interest through the semi-transparent anode. After passing through the semi-transparent organic layers and reflecting off of the Al cathode, the light is focused onto a Thorlabs DET36a biased photodetector. A transimpedance amplifier from Judson Technologies with a gain of 10^5 V/A and a 10kHz bandwidth is also used to amplify the signal. A Stanford Research SR830 lock-in amplifier is used to detect the changes in transmission. An Aligent arbitrary wavefunction generator is used to provide a dc bias superimposed on a reference ac bias of frequency 829 Hz and 0.2 V peak-to-peak amplitude. The bias scans of the EA signal were recorded under illumination with 702 nm light, which corresponds to the largest peak in the measured EA spectrum. When extrapolating the data, the zero-level crossing indicates their built-in potentials.

Supporting Information

Supporting Information is available from the Wiley Online Library or from the author.

Acknowledgements

The authors gratefully acknowledge the AFOSR (FA9550-09-1-0320) for financial support. K.R.G. and R.S. acknowledge the University Alumni Awards Program for a fellowship. The authors acknowledge the Major Analytical Instrumentation Center, Department of Materials Science and Engineering, University of Florida, for TEM, XPS, and FIB facility use. They acknowledge Eric Lambers for his assistance with XPS measurements.

Received: October 21, 2011
Revised: March 19, 2012
Published online: July 3, 2012

[1] G. Yu, J. Gao, J. C. Hummelen, F. Wudl, A. J. Heeger, *Science* **1995**, *270*, 1789.
[2] C. J. Brabec, N. S. Sariciftci, J. C. Hummelen, *Adv. Funct. Mater.* **2001**, *11*, 15.
[3] W. Ma, C. Yang, X. Gong, K. Lee, A. J. Heeger, *Adv. Funct. Mater.* **2005**, *15*, 1617.
[4] H.-Y. Chen, J. Hou, S. Zhang, Y. Liang, G. Yang, Y. Yang, L. Yu, Y. Wu, G. Li, *Nat. Photonics* **2009**, *3*, 649.
[5] T.-Y. Chu, J. Lu, S. Beaupre, Y. Zhang, J.-R. Pouliot, S. Wakim, J. Zhou, M. Leclerc, Z. Li, J. Ding, Y. Tao, *J. Am. Chem. Soc.* **2011**, *133*, 4250.
[6] H. Zhou, L. Yang, A. C. Stuart, S. C. Price, S. Liu, W. You, *Angew. Chem. Int. Ed.* **2011**, *50*, 2995.
[7] C. E. Small, S. Chen, J. Subbiah, C. M. Amb, S. W. Tsang, T. H. Lai, J. R. Reynolds, F. So, *Nat. Photonics* **2012**, *6*, 115
[8] B. Walker, A. B. Tomayo, X. D. Dang, P. Zalar, J. H. Seo, A. Garcia, M. Tantiwiwat, T. Q. Nguyen, *Adv. Funct. Mater.* **2009**, *19*, 3063.
[9] H. Shang, H. Fan, Y. Liu, W. Hu, Y. Li, X. Zhan, *Adv. Mater.* **2011**, *23*, 1554.
[10] S. Loser, C. J. Bruns, H. Miyauchi, R. P. Ortiz, A. Facchetti, S. I. Stupp, T. J. Marks, *J. Am. Chem. Soc.* **2011**, *133*, 8142.
[11] Y. Sun, G. C. Welch, W. L. Leong, C. J. Takacs, G. C. Bazan, A. J. Heeger, *Nat. Mater.* **2012**, *11*, 44.
[12] H. Hoppe, M. Niggemann, C. Winder, J. Kraut, R. Hiesgen, A. Hinsch, D. Meissner, N. S. Sariciftci, *Adv. Funct. Mater.* **2004**, *14*, 1005.
[13] J. C. Bijleveld, V. S. Gevaerts, D. D. Nuzzo, M. Turbiez, S. G. J. Mathijssen, D. M. de Leeuw, M. M. Wienk, R. A. J. Janssen, *Adv. Mater.* **2010**, *22*, E242.
[14] K. M. Coakley, M. D. McGehee, *Chem. Mater.* **2004**, *16*, 4533.
[15] S. Gunes, H. Neugebauer, N. S. Sariciftci, *Chem. Rev.* **2007**, *107*, 1324.
[16] S. E. Shaheen, C. J. Brabec, N. S. Sariciftci, F. Padinger, T. Fromherz, J. C. Hummelen, *Appl. Phys. Lett.* **2001**, *78*, 841.
[17] B. Walker, A. Tamayo, D. T. Duong, X.-D. Dang, C. Kim, J. Granstrom, T.-Q. Nguyen, *Adv. Energy Mater.* **2011**, *1*, 221.
[18] G. Li, Y. Yao, H. Yang, V. Shrotriya, G. Yang, Y. Yang, *Adv. Funct. Mater.* **2007**, *17*, 1636.
[19] S. Miller, G. Fanchini, Y. Y. Lin, C. Li, C. W. Chen, W. F. Su, M. Chhowalla, *J. Mater. Chem.* **2008**, *18*, 306.
[20] H. Y. Chen, H. C. Yang, G. W. Yang, S. Sista, R. B. Zadoyan, G. Li, Y. Yang, *J. Phys. Chem. C* **2009**, *113*, 7946.
[21] Y. Yao, J. H. Hou, Z. Xu, G. Li, Y. Yang, *Adv. Funct. Mater.* **2008**, *18*, 1783.
[22] T. Salim, L. H. Wong, B. Brauer, R. Kukreja, Y. L. Foo, Z. Bao, Y. M. Lam, *J. Mater. Chem.* **2011**, *21*, 242.
[23] F. C. Chen, H. C. Tseng, C. J. Ko, *Appl. Phys. Lett.* **2008**, *92*, 103316.
[24] J. K. Lee, W. L. Ma, C. J. Brabec, J. Yuen, J. S. Moon, J. Y. Kim, K. Lee, G. C. Bazan, A. J. Heeger, *J. Am. Chem. Soc.* **2008**, *130*, 3619.
[25] J. Peet, J. Y. Kim, N. E. Coates, W. L. Ma, D. Moses, A. J. Heeger, G. C. Bazan, *Nat. Mater.* **2007**, *6*, 497.
[26] M. Dante, A. Garcia, T. Q. Nguyen, *J. Phys. Chem. C* **2009**, *113*, 1596.
[27] Y. Liang, Z. Xu, J. Xia, S.-T. Tsai, Y. Wu, G. Li, C. Ray, L. Yu, *Adv. Mater.* **2010**, *22*, E135.
[28] H. J. Fan, H. X. Shang, Y. F. Li, X. W. Zhan, *Appl. Phys. Lett.* **2010**, *97*, 133302.
[29] K. R. Graham, J. Mei, R. Stalder, J. W. Shim, H. Cheun, F. Steffy, F. So, B. Kippelen, J. R. Reynolds, *ACS Appl. Mater. Interfaces* **2011**, *3*, 1210.
[30] C. M. Hansen, *Hansen Solubility Parameters: A User's Handbook*, CRC Press, Boca Raton, FL **2000**.
[31] A. F. M. Barton, *CRC handbook of solubility parameters and other cohesion parameters* 2nd ed., CRC Press, Boca Raton, FL **1991**.
[32] S. Walheim, M. Boltau, J. Mlynek, G. Krausch, U. Steiner, *Macromolecules* **1997**, *30*, 4995.
[33] J. Hildebrand, R. L. Scott, *The Solubility of Nonelectrolytes*, 3rd ed., Reinhold, New York **1950**.
[34] C. M. Hansen, *J. Paint Technol.* **1967**, *39*, 104.
[35] C. M. Hansen, A. L. Smith, *Carbon* **2004**, *42*, 1591.
[36] C. M. Hansen, *Hansen Solubility Parameters: A User's Handbook,* 2nd ed., CRC Press, Boca Raton, FL **2007**.
[37] M. L. Huggins, *J. Chem. Phys.* **1941**, *9*, 440.
[38] P. J. Flory, *J. Chem. Phys.* **1942**, *10*, 51.
[39] M. T. Rispens, A. Meetsma, R. Rittberger, C. J. Brabec, N. S. Sariciftci, J. C. Hummelen, *Chem. Commun.* **2003**, 2116.
[40] J. Mei, K. R. Graham, R. Stalder, J. R. Reynolds, *Org. Lett.* **2010**, *12*, 660.
[41] P. Brown, D. Thomas, A. Köhler, J. Wilson, J.-S. Kim, C. Ramsdale, H. Sirringhaus, R. Friend, *Phys. Rev. B* **2003**, *67*, 064203.
[42] M. Sundberg, O. Inganäs, S. Stafstrom, G. Gustafsson, B. Sjogren, *Solid State Commun.* **1989**, *71*, 435.
[43] J. Peet, N. S. Cho, S. K. Lee, G. C. Bazan, *Macromolecules* **2008**, *41*, 8655.
[44] J. W. Cahn, *J. Chem. Phys.* **1965**, *42*, 93.
[45] F. Brochard, J. Jouffroy, P. Levinson, *Macromolecules* **1983**, *16*, 1638.
[46] C. R. Brundle, H. Hopster, J. D. Swalen, *J. Chem. Phys.* **1979**, *70*, 5190.
[47] C. D. Bain, G. M. Whitesides, *J. Phys. Chem.* **1989**, *93*, 1670.
[48] M. P. Seah, S. J. Spencer, *Surf. Interface Anal.* **2010**, *43*, 744.
[49] H. Wang, E. D. Gomez, J. Kim, Z. Guan, C. Jaye, D. A. Fischer, A. Kahn, Y.-L. Loo, *Chem. Mater.* **2011**, *23*, 2020.
[50] S. Yamakawa, K. Tajima, K. Hashimoto, *Org. Electron.* **2009**, *10*, 511.
[51] T. Nishizawa, H. K. Lim, K. Tajima, K. Hashimoto, *Chem. Commun.* **2009**, 2469.
[52] J. Hwang, F. Amy, A. Kahn, *Org. Electron.* **2006**, *7*, 387.
[53] T. W. Lee, Y. S. Chung, *Adv. Funct. Mater.* **2008**, *18*, 2246.
[54] N. Koch, A. Vollmer, A. Elschner, *Appl. Phys. Lett.* **2007**, *90*, 043512.
[55] A. Moujoud, S. H. Oh, H. S. Shin, H. J. Kim, *Phys. Status Solidi A* **2010**, *207*, 1704.
[56] D. J. D. Moet, P. de Bruyn, P. W. M. Blom, *Appl. Phys. Lett.* **2010**, *96*, 153504.
[57] S. Nishino, J. Okada, K. Kumazawa, T. Mori, *Jpn. J. Appl. Phys., Part 1* **2007**, *46*, 7427.
[58] J. S. Huang, P. F. Miller, J. S. Wilson, A. J. de Mello, J. C. de Mello, D. D. C. Bradley, *Adv. Funct. Mater.* **2005**, *15*, 290.
[59] M. S. Kim, S. K. Park, Y. H. Kim, J. W. Kang, J. I. Han, *J. Electrochem. Soc.* **2009**, *156*, H782.
[60] H. Frohne, S. E. Shaheen, C. J. Brabec, D. C. Muller, N. S. Sariciftci, K. Meerholz, *ChemPhysChem* **2002**, *3*, 795.
[61] M. F. Lo, T. W. Ng, T. Z. Liu, V. A. L. Roy, S. L. Lai, M. K. Fung, C. S. Lee, S. T. Lee, *Appl. Phys. Lett.* **2010**, *96*, 113303.

[62] I. H. Campbell, T. W. Hagler, D. L. Smith, J. P. Ferraris, *Phys. Rev. Lett.* **1996**, *76*, 1900.
[63] M. Liess, S. Jeglinski, Z. V. Vardeny, M. Ozaki, K. Yoshino, Y. Ding, T. Barton, *Phys. Rev. B* **1997**, *56*, 15712.
[64] S. J. Martin, G. L. B. Verschoor, M. A. Webster, A. B. Walker, *Org. Electron.* **2002**, *3*, 129.
[65] B. Zimmermann, M. Glatthaar, M. Niggemann, M. Riede, A. Hinsch, *Thin Solid Films* **2005**, *493*, 170.
[66] J. Meyer, R. Khalandovsky, P. Görrn, A. Kahn, *Adv. Mater.* **2010**, *23*, 70.
[67] H. T. Nicolai, G. A. H. Wetzelaer, M. Kuik, A. J. Kronemeijer, B. de Boer., P. W. M. Blom, *Appl. Phys. Lett.* **2010**, *96*, 172107.
[68] L. Bozano, S. A. Carter, J. C. Scott, G. G. Malliaras, P. J. Brock, *Appl. Phys. Lett.* **1999**, *74*, 1132.
[69] J. C. Scott, P. J. Brock, J. R. Salem, S. Ramos, G. G. Malliaras, S. A. Carter, L. Bozano, *Synth. Met.* **2000**, *111-112*, 289.
[70] J. Bisquert, J. M. Montero, H. J. Bolink, E. M. Barea, G. Garcia-Belmonte, *Phys. Status Solidi A* **2006**, *203*, 3762.
[71] C. M. Amb, S. Chen, K. R. Graham, J. Subbiah, C. E. Small, F. So, J. R. Reynolds, *J. Am. Chem. Soc.* **2011**, *133*, 10062.